

DESIGN AND VALIDATION OF CARBON NANOTUBE THIN FILM WIRELESS SENSORS FOR PH AND CORROSION MONITORING

Kenneth J. Loh

Jerome P. Lynch

Department of Civil & Environmental Engineering, University of Michigan, Ann Arbor, MI 48109, USA

ABSTRACT

Corrosion damage in civil, aeronautical, and mechanical systems poses significant risks to users and occupants while simultaneously burdening owners with costly repairs and maintenance. Although many different sensing technologies are available to monitor corrosion processes, many cannot be easily implemented in field environments due to requiring expensive data acquisition systems and their destructive and intrusive measurement strategies. In this study, a novel layer-by-layer assembled carbon nanotube and poly(aniline)-based nanocomposite pH sensor is developed for monitoring corrosion of metallic and reinforced concrete structures. First, the electrochemical response of the proposed nanocomposite pH sensor is characterized using time-domain two-point resistance probing measurements to validate its resistance change to different pH buffer solutions (1 to 13). Frequency-domain electrical impedance spectroscopic studies and equivalent circuit analyses confirm changes in film resistance to pH. Upon sensor characterization, these nanocomposites are directly deposited onto printed circuit board coil antennas to realize a miniature passive wireless sensor capable of being embedded within structural materials. Preliminary wireless pH sensing results are presented to demonstrate that the wireless sensor's bandwidth decreases at 3.9 kHz-pH^{-1} with increasing pH.

INTRODUCTION

Structural systems, such as buildings, bridges, and aircraft often operate in harsh environmental conditions and are subjected to extreme loading events that accelerate structural deterioration. For instance, permanent deformations, corrosion, fatigue cracking, and many other types of damage can occur throughout a system's service lifetime. However, corrosion, an electrochemical and physical process, ranks as one of the most complex, severe, and difficult to detect damage phenomenon. Furthermore, prolonged undetected corrosion can escalate to eventual catastrophic structural failure. For example, corrosion

of aircraft fuselages can cause over-stressing at rivets and formation of stress-corrosion cracks; the Aloha Airlines plane that ripped apart mid-flight in 1988 is a classic example [1]. In addition to the safety risks posed to structural users, the cost of corrosion poses a significant economic burden to society. It has been estimated that the total annual direct corrosion cost to the entire U.S. industry (*i.e.*, infrastructure, utilities, transportation, production and manufacturing, and government) in 1998 was approximately \$300 billion (or more than 3% of the gross domestic product) [2]. Similarly, the U.S. Air Force Corrosion Prevention and Control Office (AFCPCO) estimates that more than \$800 million is spent annually to maintain its existing aeronautical fleet [3]. As a result, new and robust sensing technologies capable of monitoring corrosion processes are required.

Traditionally, various types of sensing techniques including visual inspection, core sampling, half-cell potential [4], linear polarization resistance (LPR) [5], electrical impedance spectroscopy (EIS) [6], among others [7-9], have been applied to detect corrosion in reinforced concrete (*i.e.*, civil infrastructures) and aluminum structures (*e.g.*, airfoils and naval vessels). The aforementioned corrosion monitoring techniques have been validated to provide accurate corrosion measurements in the laboratory. However, they all cannot be readily implemented in field environments since measurements typically require destructive removal of structural material (*e.g.*, concrete cover to access embedded steel reinforcement) and/or expensive data acquisition systems.

Alternatively, the nondestructive evaluation (NDE) and structural health monitoring (SHM) community has begun to explore the development of low-cost embeddable corrosion sensors. The main objective is to develop miniature sensors capable of being embedded during construction to measure parameters indicative of corrosion (*e.g.*, moisture, chloride ingress, pH, dissolved ions, among many others) throughout structural service lifetimes. For example, Fuhr and Huston [10] have developed a specie-independent fiber optic sensor that can

be embedded in concrete to detect corrosion of steel reinforcement by passing broadband light into an optical fiber while monitoring color modulation. Results presented indicate that measured peak wavelengths correlate with changes in electrical current flowing through steel during accelerated corrosion tests. In order to realize the detection of corrosion at multiple locations on a large structural system and to prevent embedding long lengths of cables (or optical fibers), Watters [11] and Watters, *et al.* [12] have developed a passive wireless corrosion sensor operating at 125 kHz. Using radio frequency identification (RFID) technology, power can be wirelessly transmitted to the embedded Smart Pebble, and the sensor is then commanded to measure chloride concentration and/or temperature. Similarly, Dickerson, *et al.* [13] have also designed a prototype passive wireless sensor that exhibits change in resonant frequency when corrosion exceeds a predetermined threshold.

As mentioned earlier, while various structural parameters such as humidity, chloride concentration, pH, temperature, among others can be used to predict the onset of corrosion, ambient pH has been shown to be an accurate and reliable corrosion indicator. For instance, aluminum alloys used for aerospace structures undergo high corrosion rates when subjected to highly acidic or alkaline environments [14]; on the other hand, steel reinforcement used in civil infrastructures is normally resistant against corrosion due to concrete's inherent high alkalinity (pH > 13.5) but becomes vulnerable to corrosion when ambient pH levels fall below 9 [9]. Thus, an effective way to monitor corrosion of structural systems is to employ specie-independent pH sensors.

In this study, processing tools from the nanotechnology domain are employed to molecularly design thin film composites exhibiting electrochemical response to pH. As opposed to the miniaturization of macro-scale sensor designs, nanofabrication tools such as the layer-by-layer (LbL) self-assembly technique can deposit functional nanomaterials and polyelectrolytes that exhibit high mechanical strength, chemical resistance (to survive harsh environmental conditions), and electrical sensitivity to pH. In addition, these nanometer-thick films can be coated onto structural surfaces (*e.g.*, airfoils) or embedded within concrete and composites without interfering with structural performance. Here, single-walled carbon nanotubes (SWNT) and conductive polymers such as poly(aniline) (PANI) are employed for the design of pH-sensitive nanocomposites [15, 16]. By designing nanocomposites with a large sensing range (pH 1 to 14), these thin films are applicable for corrosion monitoring of various materials including concrete and metallic (*e.g.*, aluminum) structures.

Since corrosion damage can occur at any location in a large structural system, low-cost and densely-distributed sensors are required to identify the location and severity of corrosion damage. Thus, nanocomposites are directly assembled onto printed circuit board (PCB) coil antennas to realize passive wireless sensing capabilities. By taking advantage of radio frequency identification technology, no batteries are required to

power embedded sensor tags; instead, a portable reader can wirelessly transmit power to sensors while simultaneously obtaining sensor output data.

This paper begins with a brief theoretical discussion regarding the fundamental operating principles of RFID and inductively coupled devices. Then, a detailed discussion of sensor design, including the antenna design and LbL assembly process, is explained. Upon sensor fabrication, time-domain two-point electrical resistance measurements and frequency-domain electrical impedance spectroscopy are employed to characterize SWNT-based nanocomposite pH sensing performance. Finally, preliminary laboratory results are presented to show changes in sensor bandwidth as a function of the applied pH buffer solution.

INDUCTIVE COUPLING BACKGROUND

In general, near-field radio frequency identification (or more generally, inductively coupled systems) are comprised of two main components: (1) a reader connected to a constant power source and (2) a passive sensor tag. The reader serves as the data acquisition system (DAQ) and is responsible for wirelessly transmitting power to an RFID tag in close proximity via inductive coupling [17]. When the sensor tag is interrogated by an RFID reader, simple onboard computations can take place before the sensor tag transmits data back (or uplinks) to the reader base station using techniques such as amplitude (ASK), frequency (FSK), or phase shift keying (PSK) [18]. To date, RFID has found applications in smart cards, security systems, package tracking, sensors, among many others.

RFID Reader

Typically, the RFID reader consists of a coil antenna (*i.e.*, an inductor, L_R) connected to an automated frequency response analyzer (FRA) such as the Solartron 1260 impedance gain/phase analyzer used in this study. Here, the Solartron impedance analyzer passes an alternating current (AC) of regulated voltage (of the form $P(t) = V_0 \sin(\omega t)$, where V_0 is the voltage amplitude and $\omega = 2\pi f$ is the natural cyclic frequency of AC current) while simultaneously measuring current (I) and phase shift (θ) to determine the reader antenna's complex impedance ($Z = Z' + iZ''$). The applied AC signal frequency (f) is then varied and can range from 100 mHz to 32 MHz in order to measure the frequency-impedance response of the RFID system. Furthermore, when an AC current is passed through the reader coil, a magnetic field of magnitude H is generated as shown in Equation 1:

$$H = \frac{I \cdot N \cdot r^2}{2\sqrt{(r^2 + x^2)^3}} \quad (1)$$

where r is the antenna radius, N is the number of turns, and x is the read-distance along the central axis of the coil [17]. The generated magnetic field is employed to wirelessly communicate and transmit power to sensor tags in close proximity as shown schematically in Figure 1.

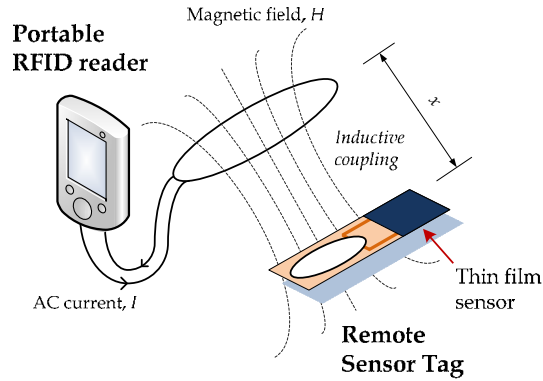


Figure 1. A schematic illustrating reader and sensor tag inductive coupling.

Sensor Tag or Transponder

One of the main advantages of radio frequency identification systems is that sensor tags do not require a constant power supply (*e.g.*, batteries or AC power), thereby permitting the design of miniature thin film tags capable of being embedded in structures. The design of the simplest sensor tag consists of a resistor (R_T), inductor (coil antenna) (L_T), and capacitor (C_T) arranged in a series or parallel resonant circuit configuration (termed an RLC-circuit). Each RLC-circuit is characterized by two inherent properties, namely its characteristic (or resonant) frequency (f_n) and bandwidth (B). While the characteristic frequency does not vary between tag circuitry, bandwidth varies between a parallel and series resonant circuit as shown in Equations (2) and (3) [19]:

$$f_n = \frac{1}{2\pi\sqrt{L_T C_T}} \quad (2)$$

$$B_{series} = \frac{R_T}{2\pi L_T} \quad (3a)$$

$$B_{parallel} = \frac{1}{2\pi R_T C_T} \quad (3b)$$

Selection of the tag circuit configuration (series versus parallel) depends on whether shifts in characteristic frequency or changes in bandwidth are more desirable and whether the sensing mechanism is based on inductive, resistive, and/or capacitive changes. In this study, a parallel resonant circuit is selected to respond to varying pH by changing system bandwidth.

Coupled Reader-Tag System

As mentioned earlier, reader impedance is measured experimentally using a Solartron 1260 impedance gain/phase analyzer. Equivalent circuit analysis allows the impedance of the reader to be expressed as Equation 4:

$$Z(\omega) = R_R + j\omega L_R \quad (4)$$

such that R_R is the inherent series resistance of the reader coil antenna, and ω (in rad-s⁻¹) is the input AC signal's natural

cyclic frequency corresponding to measured impedance. However, when a sensor tag approaches the detectable range, the reader's complex impedance response (Equation 4) is disrupted by the presence of the tag and can be modeled as an additional complex impedance term, Z_T' , due to inductive coupling (Equation 5).

$$Z(\omega) = R_R + j\omega L_R + Z_T' \quad (5)$$

The exact nature as to how a reader's complex impedance is modified by the presence of a tag depends upon whether the tag is an RLC-series or -parallel resonant circuit. For instance, the impedance measured at the reader due to inductive coupling with a series resonant circuit can be derived and calculated via Equation 6:

$$Z(\omega) = R_R + j\omega L_R + \frac{k^2 \omega^2 L_R L_T}{Z_L + Z_R + Z_C} \quad (6)$$

On the other hand, for a parallel resonant circuit:

$$Z(\omega) = R_R + j\omega L_R + \frac{k^2 \omega^2 L_R L_T}{1/Z_L + 1/Z_R + 1/Z_C} \quad (7)$$

For Equations 6 and 7, Z_L , Z_R , and Z_C correspond to the equivalent complex impedance of the sensor tag's inductor (with some inherent coil resistance R_S), resistor, and capacitor, respectively as shown in Equation 8.

$$\begin{aligned} Z_L &= R_S + j\omega L_T \\ Z_R &= R_T \\ Z_C &= 1/[j\omega C_T] \end{aligned} \quad (8)$$

From Equations 6 and 7, a coupling factor k (between 0 and 1) is included to qualitatively describe the mutual inductance between the reader and tag [17]. Under optimal conditions where the distance (x) between reader and tag is zero and when both antennas are aligned along their coil axes, $k = 1$. However, this theoretical k value is rarely achieved under normal operating conditions since the coupling factor is influenced by coil geometry, read range, ambient conditions,

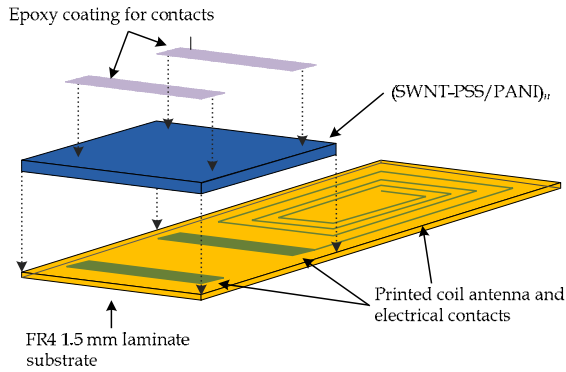


Figure 2. Multilayered approach to the deposition of nanocomposite upon a RFID printed circuit.

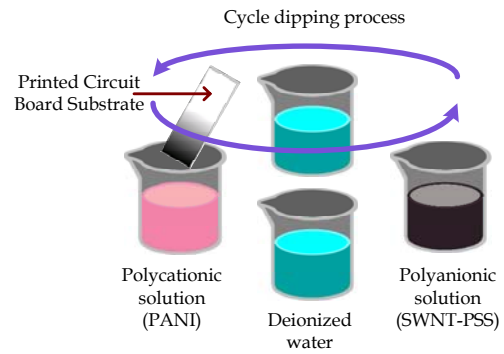
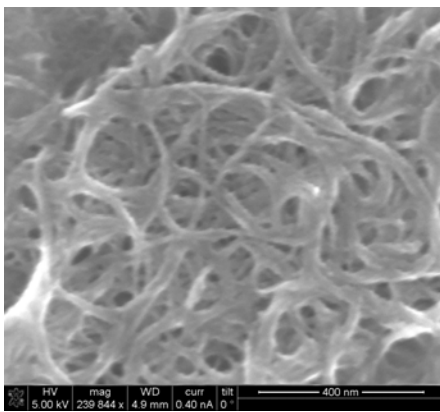
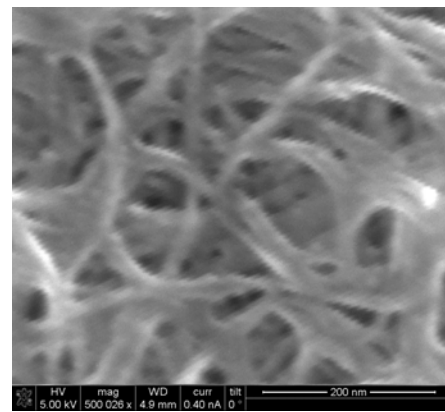


Figure 3. Rhe layer-by-layer thin film fabrication methodology.



(a)



(b)

Figure 4. SEM images of the deposition of dispersed carbon nanotube within nanocomposites imaged at (a) moderate (240,000 times) and (b) high (500,000 times) magnification.

among many other factors. Nevertheless, it should be noted that when the tag is out-of-range from the RFID reader, k becomes zero and Equations 6 and 7 reduce to Equation 4 (*i.e.*, the measured reader impedance is no longer affected by the sensor tag). Readers are referred to Finkenzeller [17] for a more detailed discussion on the fundamental operating principles of inductively coupled systems.

SENSOR FABRICATION

Coil Antenna and Substrate Fabrication

In order to take full advantage of RFID small form factors, printed circuit board technologies are employed to electroplate and pattern conductive (63/37 fused tin-lead over copper) coil antennas onto 1.5 mm thick FR4 laminates (by AP Circuits, Inc.). Here, a five-turn square coil antenna with a maximum outer dimension of 23 mm and a coil trace width of 0.4 mm is designed to realize a 2.6 μH inductor. These PCB coil antennas can then be coupled with a nanocomposite pH sensor (as the tag resistor) and a 1,000 pF or 1,500 pF leaded ceramic capacitor to achieve a desired tag resonant frequency of 3.0 or 2.5 MHz, respectively (as calculated from Equation 1) (Figure

2). In addition, a thin epoxy coating is applied over regions where the film is deposited onto PCB electrical contacts.

Layer-by-Layer Nanocomposite Assembly

While many different thin film fabrication techniques have been developed (*e.g.*, spin coating, vacuum filtration, melt-pressing and annealing, among others), layer-by-layer self-assembly permits the homogeneous deposition of nanomaterials and polyelectrolyte species onto virtually any substrate and geometry. In short, LbL is performed by sequentially immersing a charged substrate (*e.g.*, glass metal, polymers, or FR4 laminates) into oppositely charged solutions containing functional nanomaterials (Figure 3). When exposed to each solution, electrostatic and van der Waals force interactions drive the adsorption of various materials to form nanometer-thick monolayer thin films [20]. Through the continuous repetition of this cyclic adsorption process, a variety of materials such as individually dispersed carbon nanotubes and poly(aniline) can be incorporated to yield nanocomposites encoded with specific engineering functionalities [20, 21]. Scanning electron microscope (SEM) images of LbL-assembled carbon nanotube composites verify the adsorption of

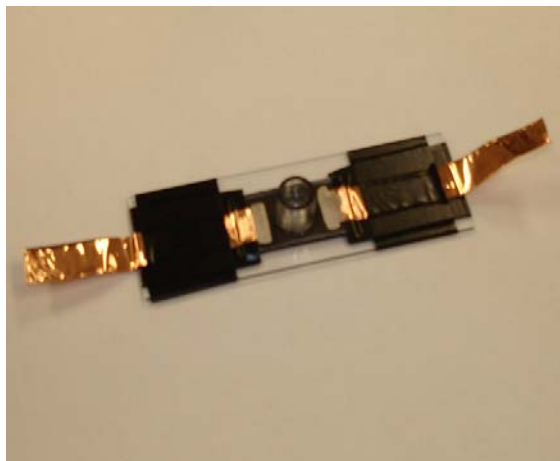


Figure 5. A two-point probe setup using copper tape and silver paste is electrically connected to a (SWNT-PSS/PANI)₅₀ specimen for time-domain resistance measurement as a function of pH.

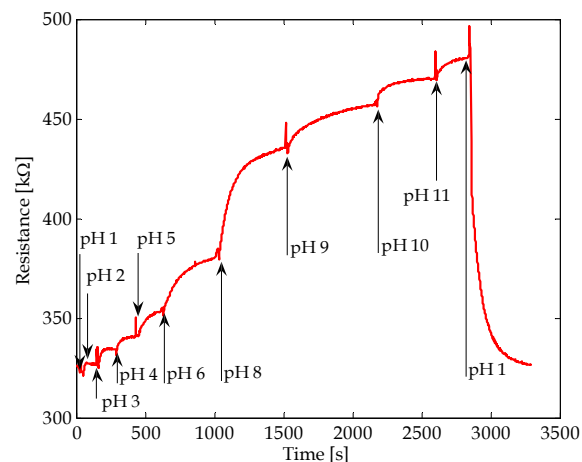


Figure 6. The two-point probe time history response of a (SWNT-PSS/PANI)₅₀ thin film subjected to pH 1 to 11 buffer solutions.

individual or small bundles of carbon nanotubes within the polymeric matrix (Figure 4).

More specifically, prior to LbL assembly, printed circuit boards (FR4 laminates) are thoroughly rinsed and cleansed with 18 MΩ deionized water (Milli-Q). Nanocomposite assembly begins by dipping the FR4 laminate in a positively charged 1.0 mg·mL⁻¹ poly(aniline) emeraldine base solution in 10 vol. % N,N-dimethyl formamide (DMF) for 5 min. Then, the FR4 substrate, along with its adsorbed monolayer, are rinsed with 18 MΩ deionized water (3 min) to remove loosely adsorbed polyelectrolytes and dried using compressed air for 10 minutes. Deposition of the next oppositely charged LbL counterpart continues by immersing the substrate into a solution consisting of 0.8 mg·mL⁻¹ SWNTs ultrasonically dispersed in 1.0 wt. % poly(sodium 4-styrene sulfonate) (PSS, $M_w = 1,000,000$). Previous studies conducted by Loh, *et al.* [16, 22] have validated the dispersion quality of nanotubes in polyelectrolyte solutions such as PSS. Finally, upon rinsing (3 min) and drying (10 min), one bilayer of (SWNT-PSS/PANI)₁ thin film is deposited onto the FR4 laminate substrate (where the subscript indicates the number of bilayers fabricated). Typically, the LbL technique is repeated 50 to 200 times to fabricate mechanically strong and chemically resistant thin films capable of withstanding exposure to multiple cycles of highly acidic and alkaline solutions.

NANOCOMPOSITE SENSOR CHARACTERIZATION

Time-Domain pH Sensing Characterization

Initially, demonstration of (SWNT-PSS/PANI)_n thin films' electrochemical sensitivity to applied pH buffer solutions is accomplished by depositing 50-bilayer LbL thin films upon a

clean glass substrate. Copper tape (Ted Pella) electrodes are affixed onto two ends of the (SWNT-PSS/PANI)₅₀ thin film to achieve a two-point probe setup. In addition, contact impedance is minimized by applying colloidal silver paste (Ted Pella) over the copper tape and nanocomposite. Then, a plastic well (7 mm diameter) is securely mounted over the thin film surface via vacuum grease (Dow Corning). Changes in thin film electrical resistance due to pH buffer solutions added to the well is measured with an Agilent 34401a digital multimeter supplying 10 nA of direct current (DC) while sampling at 1 Hz.

Figure 6 plots the time history of the thin film resistance to applied pH buffer solutions. Initially, the thin film is exposed to a pH 1 buffer solution. Upon observing steady-state resistance output, the buffer solution is removed at which point the next pH buffer solution is pipetted into the well. From Figure 6, it can be observed that the (SWNT-PSS/PANI)₅₀ nanocomposite exhibits dramatic changes in resistance as a function of pH. More importantly, upon pipetting in a pH 11 solution, the immediate addition of fresh pH 1 solution causes the film resistance to decrease back to the film's nominal resistance, thereby suggesting that the nanocomposite response is repeatable. Changes in film conductivity (the inverse of resistivity) are due to deprotonation of the aniline chains embedded within the nanocomposite.

Frequency-Domain pH Sensing Characterization

While DC time-domain electrical characterization has already revealed the high sensitivity of (SWNT-PSS/PANI)_n nanocomposite's resistivity to pH, frequency-domain evaluation can reveal other changes in the film's electrical properties (*e.g.*, capacitance or inductance). In fact, the Solartron 1260 impedance gain/phase analyzer can be

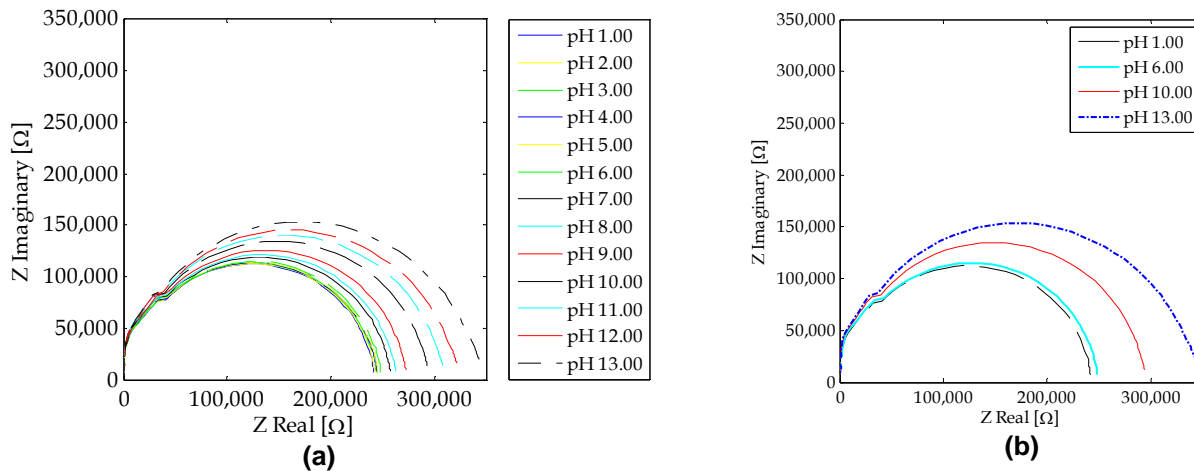


Figure 7. Electrical impedance spectroscopic plots showing the (SWNT-PSS/PANI)₅₀ thin films increase their parallel resistance with increasing pH (pH 1 to 13).

employed to conduct electrical impedance spectroscopy for characterizing frequency-domain electrical properties of the proposed nanocomposites [24]. As opposed to measuring a reader coil antenna's complex impedance, the FRA is directly connected to the thin film specimen shown in Figure 5. By applying a regulated AC voltage signal of the form $P(t) = V_0 \sin(\omega t)$, the measured steady-state current response of the form $i(t) = \sin(\omega t + \theta)$ (where θ is the phase difference between the input and output AC signals) is employed to determine the specimen's complex impedance. Then, the Solartron impedance analyzer is commanded to measure nanocomposite impedance between applied AC signal frequencies from 1 to 10 MHz. Upon determination of thin film complex impedance at every frequency interval, the real and imaginary components of $Z(\omega)$ can be calculated using Equation 9:

$$Z_{Real} \equiv Z' = \|Z\| \cos(\theta) \quad (9a)$$

$$Z_{Imaginary} \equiv Z'' = \|Z\| \sin(\theta) \quad (9b)$$

Figure 7 plots the experimental response of EIS measurements of an (SWNT-PSS/PANI)₅₀ nanocomposite subjected to buffer solutions ranging from pH 1 to 13. The semicircular thin film EIS response in the complex impedance plane (termed the Cole-Cole plot) suggests that these thin films exhibit a resistor-capacitor (RC) parallel circuit-type behavior (Figure 8) [24]. It is expected that an increase in the Cole-Cole semicircular plot radius with increasing pH suggests an increase in resistance of the parallel-RC circuit.

Thus, each Cole-Cole plot is numerically fitted to an equivalent circuit schematically shown in Figure 8 using a stochastic simulated annealing model-updating algorithm to deduce values for the equivalent resistance and capacitance of the (SWNT-PSS/PANI)₅₀ nanocomposite pH sensor. Similar equivalent circuit analysis of carbon nanotube-based composites has been conducted and validated by Loh, *et al.*

[22] and Kang, *et al.* [25]. Upon model-fitting of EIS thin film response to applied pH buffer solutions, the results are summarized as shown in Figure 9. The LbL thin film's frequency-domain equivalent resistance exhibits a bilinear response to pH, where lower sensitivity is observed for acidic pH solutions ($1 \text{ k}\Omega\text{-pH}^{-1}$) but dramatically increases when exposed to basic solutions ($15 \text{ k}\Omega\text{-pH}^{-1}$ as shown in Figure 9). It should be noted that no obvious trends are identified for capacitance change with varying pH but rather remains constant at 1.7 pF. These results suggest a parallel resonant circuit configuration can achieve maximum RFID bandwidth change as a function of pH (Equation 3b).

PASSIVE WIRELESS PH SENSING

In a previous study conducted by Loh, *et al.* [26], nanocomposite strain and pH sensors have been coupled with 45 and 70 mm coil antennas formed from wound magnetic wire for validating passive wireless sensing and communications. Preliminary results indicate that an RFID reader can interrogate these sensors and detect system bandwidth change due to applied strain ($\pm 10,000 \mu\epsilon$) or pH (1 to 10). However, the large form factor of these coil antennas makes them unrealistic for embedding within structural components. As a result, the main objective of this study is to take advantage of the versatility of LbL to deposit nanocomposite sensors on substrates such as PCB planar coil antennas. The end result is a thin and compact pH/corrosion RFID sensor tag that is suitable for embedding in structural materials such as reinforced concrete (Figure 10).

In this study, realization of the RFID reader is achieved by coupling a PCB coil antenna ($\sim 2.6 \mu\text{H}$) with the Solartron 1260 impedance gain/phase analyzer. The FRA is programmed to apply an AC sinusoidal excitation (regulated 3V voltage) from 1.5 to 5.5 MHz to interrogate the proposed sensor tag while simultaneously measuring changes in the reader's complex

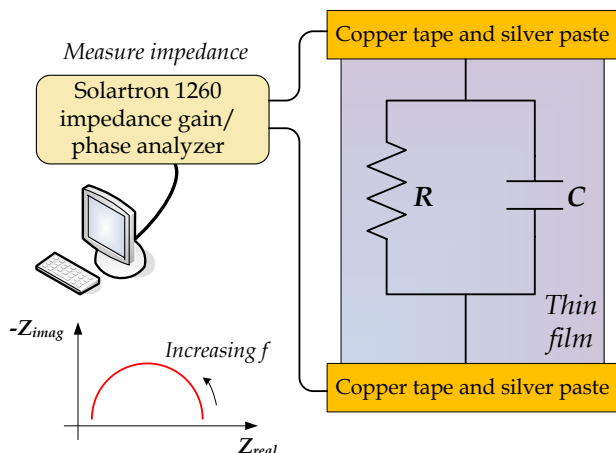


Figure 8. An equivalent parallel-RC circuit model is derived for simulated annealing model-fitting of nanocomposite EIS Cole-Cole plot response.

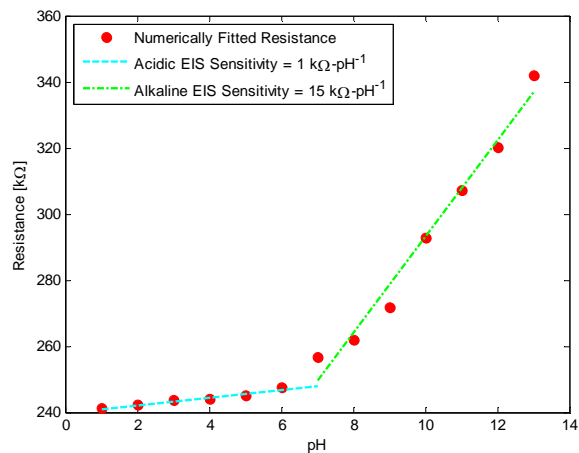


Figure 9. A plot of model-fitted equivalent circuit resistance as a function of applied pH buffer solutions indicating bilinear pH sensitivity.

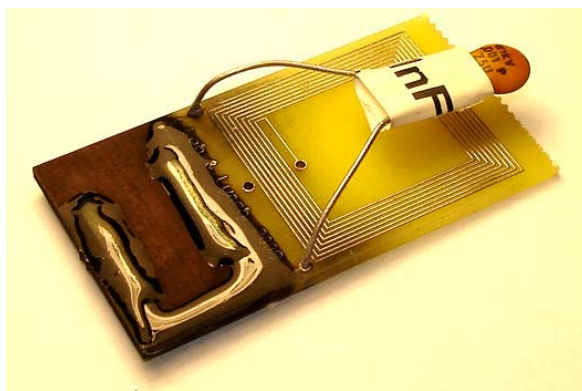


Figure 10. Layer-by-layer assembly is employed to deposit (SWNT-PSS/PANI)₅₀ thin films directly onto PCB coil antennas to realize a passive wireless RFID pH/corrosion sensor tag of small form factor.

impedance. For the sensor tag shown in Figure 10, a 1,000 pF leaded ceramic capacitor is soldered to the PCB substrate to tune the resonant frequency to ~ 3.0 MHz and bandwidth to ~ 250 kHz. Laboratory validation of passive wireless pH sensing is conducted by exposing the nanocomposite-coated portion of the tag (Figure 10) to buffer solutions of various pH levels (pH 1 to 11). It should be noted that strong bases are avoided in this preliminary study while FR4 laminate chemical resistance tests are currently underway. In addition, the reader and tag are aligned at their coil axes and are separated by 5 to 15 mm.

Figure 11 plots the passive wireless pH sensor's impedance-frequency response (termed a Bode plot) as determined by the RFID reader. It should be noted that only select plots are presented to enhance the clarity of the printed figure. From Figure 11, it can be clearly seen that inductive coupling between the reader and tag is observed near the sensor tag's 3.0 MHz characteristic frequency as expected. As the sensor tag is exposed to increasing alkaline pH buffer solutions

(1 to 11), the maximum detected impedance magnitude decreases while the bandwidth of the reader-tag system increases; Figure 12 summarizes system bandwidth dependency to applied pH. Thus, as the nanocomposite's resistance increases with increasing pH (Figures 9), RFID bandwidth decreases in accordance with Equation 3b. Although bandwidth change is nonlinearly related to pH, a linear least-squares fit can be obtained to estimate the inductively coupled sensor sensitivity to be 3.9 kHz·pH⁻¹. This high estimated pH sensitivity suggests that these passive wireless sensors hold promise for applications in field environments to monitor corrosion.

As mentioned earlier, the sensor tag's FR4 laminates are currently being evaluated to endure harsh environmental conditions (strong acids and bases). In the near future, the sensor tag and reader coil antenna will be optimized to further enhance sensor read range and system bandwidth change. Moreover, these nanocomposite PCB RFID tags have already

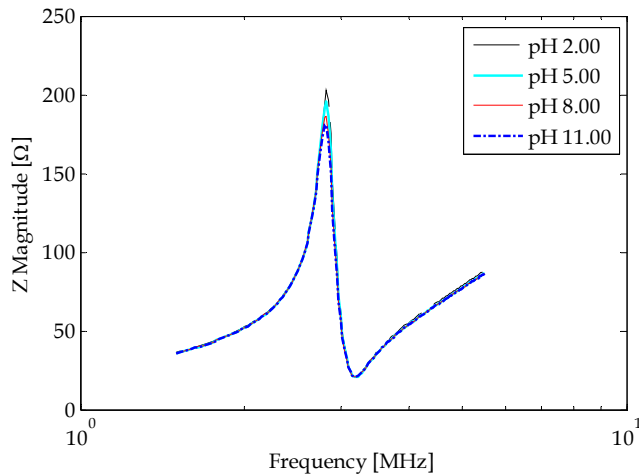


Figure 11. Select Bode plots measured by the RFID reader are presented to illustrate sensor response to various applied pH buffer solutions.

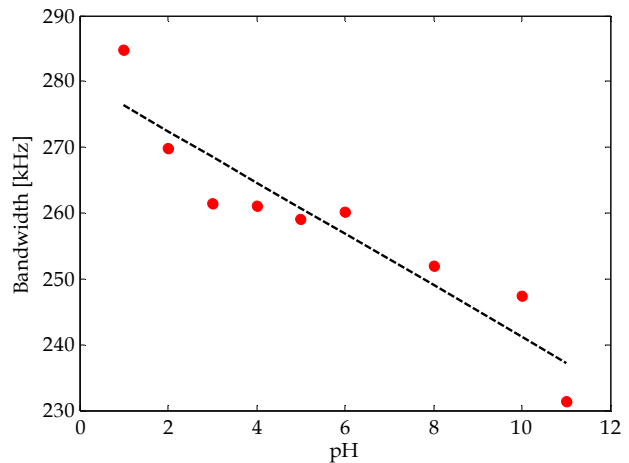


Figure 12. The RFID system bandwidth decreases with increasing pH buffer solutions; the sensitivity of the proposed system is approximately 3.9 kHz-pH^{-1} .

been embedded within reinforced concrete structures to detect corrosion (pH changes) during accelerated corrosion tests.

CONCLUSIONS

A (SWNT-PSS/PANI)_n layer-by-layer nanocomposite has been proposed for pH and corrosion monitoring. Extensive DC time-domain and AC frequency-domain studies have been conducted to evaluate sensor performance to detect pH buffer solutions from pH 1 to 13. Results from DC two-point probe resistance measurements, AC electrical impedance spectroscopy, and equivalent circuit analyses have confirmed that thin film resistance increases in tandem with increasingly applied pH buffer solutions. However, the sensor does exhibit bilinear sensitivity to pH, such that the nanocomposite is only moderately sensitive to acidic solutions, but its electrical resistance can increase dramatically in alkaline environments.

Upon sensor characterization, passive wireless sensing is accomplished by directly depositing these thin film pH sensors onto PCB coil antennas. Wireless interrogation has been successfully validated to detect sensor tags tuned to a 3.0 MHz characteristic frequency and 250 kHz bandwidth. When these RFID tags are exposed to pH buffer solutions (pH 1 to 11), the sensor's bandwidth decreases with increasing pH, exhibiting a pH sensitivity of 3.9 kHz-pH^{-1} . The results presented show promise for passive wireless pH detection for structural health monitoring. Work is underway to embed these passive wireless sensors in reinforced concrete structures to detect environmental parameters conducive to steel-reinforcement corrosion.

ACKNOWLEDGMENTS

The authors would like to thank the National Science Foundation (NSF Grant No. CMMI-0528867 under Dr. S. C. Liu) for support of this research.

REFERENCES

- [1] Samsonov, P., 1993, "Nondestructive inspection of aging aircraft," Proceedings of *SPIE*, **2001**, pp. 257-261.
- [2] Koch, G. H., Brongers, M. P. H., Thompson, M. G., Virmani, Y. P. and Prayer, J. H., 2001, "Corrosion cost and preventive strategies in the united states," FHWA-RD-01-156, Federal Highway Administration (FHWA), Department of Transportation (DOT), McLean, VA, pp. 1-16.
- [3] Bullock, D. and Anderl, T., 2004, "Corrosion prevention and control office," Proceedings of *ARFL Horizons*, pp.
- [4] Dhir, R. K., Jones, M. R. and McCarthy, M. J., 1993, "Quantifying chloride-induced corrosion from half-cell potential," *Cement and Concrete Research*, **23** (6), pp. 1443-1454.
- [5] Rocchini, G., 1993, "Corrosion rate monitoring by the linear polarization method," *Corrosion Science*, **34** (12), pp. 2031-2044.
- [6] Oltra, R. and Keddad, M., 1990, "Application of eis to localized corrosion," *Electrochimica Acta*, **35** (10), pp. 1619-1629.
- [7] Ahmad, S., 2003, "Reinforcement corrosion in concrete structures, its monitoring and service life prediction - a review," *Cement & Concrete Composites*, **25** (4-5), pp. 459-471.
- [8] Broomfield, J. P., Davies, K. and Hladky, K., 2002, "The use of permanent corrosion monitoring in new and existing reinforced concrete structures," *Cement & Concrete Composites*, **24** (1), pp. 27-34.
- [9] Carino, N. J., 1999, "Nondestructive techniques to investigate corrosion status in concrete structures," *Journal of Performance of Constructed Facilities*, **13** (3), pp. 96-106.

- [10] Fuhr, P. L. and Huston, D. R., 1998, "Corrosion detection in reinforced concrete roadways and bridges via embedded fiber optic sensors," *Smart Materials and Structures*, **7** (2), pp. 217-228.
- [11] Watters, D. G., 2003, "Wireless sensors will monitor bridge decks," *Better Roads*, **73** (2), pp. 74-75.
- [12] Watters, D. G., Jayaweera, P., Bahr, A. J., Huestis, D. L., Priyantha, N., Meline, R., Reis, R. and Parks, D., 2003, "Smart pebble: Wireless sensors for structural health monitoring of bridge decks," Proceedings of *SPIE - Smart Structures and Materials*, **5057**, pp. 20-28.
- [13] Dickerson, N. P., Andringa, M. M., Puryear, J. M., Wood, S. L. and Neikirk, D. P., 2006, "Wireless threshold sensors for detecting corrosion in reinforced concrete structures," Proceedings of *SPIE - Smart Structures and Materials*, **6174**, pp.
- [14] Ambat, R. and Dwarakadasa, E. S., 1992, "The influence of ph on the corrosion of medium strength aerospace alloys 8090, 2091 and 2014," *Corrosion Science*, **33** (5), pp. 681-690.
- [15] Ferrer-Anglada, N., Kaempgen, M. and Roth, S., 2006, "Transparent and flexible carbon nanotube/polypyrrole and carbon nanotube/polyaniline ph sensors," *Physica Status Solidi B*, **243** (13), pp. 3519-3523.
- [16] Loh, K. J., Kim, J., Lynch, J. P., Kam, N. W. S. and Kotov, N. A., 2007, "Multifunctional layer-by-layer carbon nanotube-polyelectrolyte thin films for strain and corrosion sensing," *Smart Materials and Structures*, **16** (2), pp. 429-438.
- [17] Finkenzeller, K., *Rfid handbook: Fundamentals and applications in contactless smart cards and identification*, John Wiley & Sons: West Sussex, England, 2003.
- [18] Paret, D., *Rfid and contactless smart card applications*, John Wiley & Sons: West Sussex, England, 2005.
- [19] Lee, Y., 1998, "Rfid coil design," *Microchip*, AN678, pp. 1-18.
- [20] Decher, G. and Schlenoff, J. B., ed., *Multilayer thin films: Sequential assembly of nanocomposite materials*, Wiley-VCH: Federal Republic of Germany, 2003.
- [21] Decher, G., 1997, "Fuzzy nanoassemblies: Toward layered polymeric multicomposites," *Science*, **277** (29), pp. 1232-1237.
- [22] Loh, K. J., Lynch, J. P., Shim, B. S. and Kotov, N. A., 2008, "Tailoring piezoresistive sensitivity of multilayer carbon nanotube composite strain sensors," *Journal of Intelligent Material Systems and Structures*, **19** (7), pp. 747-764.
- [23] Hou, T.-C., Loh, K. J. and Lynch, J. P., 2007, "Electrical impedance tomography of carbon nanotube composite materials," Proceedings of *SPIE - Sensors and Smart Structures Technologies for Civil, Mechanical, and Aerospace Systems*, **6529**, pp. 652926/1-652926/10.
- [24] Barsoukov, E. and Macdonald, J. R., ed., John Wiley & Sons: Hoboken, NJ, 2005.
- [25] Kang, I., Schulz, M. J., Kim, J. H., Shanov, V. and Shi, D., 2006, "A carbon nanotube strain sensor for structural health monitoring," *Smart Materials and Structures*, **15** (3), pp. 734-7486.
- [26] Loh, K. J., Lynch, J. P. and Kotov, N. A., 2008, "Inductively coupled nanocomposite wireless strain and ph sensors," *Smart Structures and Systems*, **4** (5), pp. 531-548.